Valley Chern numbers and boundary modes in gapped bilayer graphene

Fan Zhang[a], Allan H. MacDonald[b,1], and Eugene J. Mele[a]

[a]Department of Physics and Astronomy, University of Pennsylvania, Philadelphia, PA 19104; and [b]Department of Physics, University of Texas at Austin, Austin, TX 78712

Contributed by Allan H. MacDonald, May 9, 2013 (sent for review January 22, 2013)

Electronic states at domain walls in bilayer graphene are studied by analyzing their four- and two-band continuum models, by performing numerical calculations on the lattice, and by using quantum geometric arguments. The continuum theories explain the distinct electronic properties of boundary modes localized near domain walls formed by interlayer electric field reversal, by interlayer stacking reversal, and by simultaneous reversal of both quantities. Boundary mode properties are related to topological transitions and gap closures, which occur in the bulk Hamiltonian parameter space. The important role played by intervalley coupling effects not directly captured by the continuum model is addressed using lattice calculations for specific domain wall structures.

topological states | topological defects | layer-stacking walls | few-layer graphene

The electronic properties of few layer graphene systems depend sensitively on the atomic registry between neighboring layers (1) with important consequences for applications in graphene-based electronics. Unlike single-layer graphene, bilayer graphene (BLG) with *AB* stacking is converted from a semimetal to a small gap semiconductor by the application of a perpendicular electric field (2–6). This occurs because (*i*) the interlayer hybridization of orbitals on eclipsed lattice sites breaks the sublattice symmetry on each layer, replacing the pseudorelativistic description of single layer graphene by a theory in which two quadratically dispersing chiral bands touch at discrete points in momentum space (2, 7), and (*ii*) the perpendicular electric field further breaks inversion symmetry, creating a semiconductor by gapping these low-energy degrees of freedom. The possibility of exploiting this type of field tunable gap is being vigorously pursued in ultraclean dual-gated devices (8–11).

It has been appreciated that this field-induced gap admits a topological interpretation (12, 13). The low-energy theory for BLG can be represented by an effective two-band model from which it is readily seen that inversion-symmetry breaking induces large momentum-space Berry curvatures (13, 14). The Berry curvatures have opposite signs near the two inequivalent Brillouin-zone corners (valleys) at which gaps are opened, so the integral of the Berry curvature over the full Brillouin zone is zero. Nonetheless, the integral of the Berry curvature within a single valley is nonzero, and this allows a topological analysis of the valley-projected electronic spectrum. This idea has been developed in a continuum analysis of the subgap electronic states bound to a BLG domain wall formed by a sign reversal of the interlayer electric field (12, 15–19). These electric-field walls (EFWs) are predicted to bind pairs of subgap chiral copropagating boundary modes, an interesting feature that can be related to the change in sign across a domain wall of a valley-projected topological index.

In this article, we examine the related BLG domain wall problem in which the interlayer electric field is uniform but the layer stacking switches from *AB* to *BA* registry. This version of the problem changes the boundary conditions for matching the electronic states of the two bounding phases and requires that we augment the two-band model of BLG (2, 12, 13) by accounting for all four of its sublattice degrees of freedom. Nonetheless, we find that layer-stacking walls (LSWs) bind electronic states with the same chiral structure as for the EFW studied previously. Here, we make this connection explicit by mapping the two problems onto each other within a family of four-band BLG Hamiltonians. Our results demonstrate that the topological transition in a LSW structure is associated with a finite momentum gap closure in the parameter space of four-band BLG Hamiltonians. We construct a phase diagram (Fig. 1) that identifies the different types of topologically protected states that are possible in BLG samples in which both the interlayer electric field and the layer stacking order vary in space. This analysis identifies yet a third type of domain wall in which the two pairs of chiral modes within a single valley are coupled, gapping the spectrum and annihilating boundary modes. Our results are supported by a continuum analysis of the domain wall states, lattice calculations for specific defect structures, and analysis using quantum geometrical arguments. Taken together, these elements provide a general framework for understanding the origin of the valley-projected topological states in BLG, and their fate in the presence of intervalley scattering.

Two-Band Continuum Formulation

The electronic states for BLG can be represented by four-component wave functions $\Psi=(\psi_{A_T},\psi_{B_T},\psi_{A_B},\psi_{B_B})$, where ψ denotes the atomic orbital centered on the A or B sites of the top or bottom layer. At low energies, the Hamiltonian can be expanded for small $\boldsymbol{q}$ around the two inequivalent Brillouin zone corners: $\mathcal{H}(\nu\boldsymbol{K}+\boldsymbol{q})$ with $\nu=\pm1$ denoting K and K'. Using Pauli matrices $\boldsymbol{\sigma}$ to represent operators that act on the sublattice degree of freedom within a layer and $\boldsymbol{\tau}$ to represent operators acting on the layer degree of freedom, the BLG Hamiltonian can separated into layer diagonal and layer off-diagonal contributions by writing $\mathcal{H}=\mathcal{H}_0+\mathcal{H}_{int}$. We find that for *AB* stacked BLG in which the A sites of top layer hybridize with the B sites of the bottom layer, $\mathcal{H}_0=\nu q_x\sigma_x\tau_0+q_y\sigma_y\tau_0$ and $\mathcal{H}_{int}=\gamma(\sigma_x\tau_x-\sigma_y\tau_y)/2$ with $\gamma=\gamma_1/\hbar v$, where energies are normalized by $\hbar v$, γ_1 is the nearest-interlayer-neighbor hopping amplitude, and v is the electron velocity in an isolated layer. For the reversed *BA* stacking order, the interlayer coupling term becomes $\mathcal{H}_{int}=\gamma(\sigma_x\tau_x+\sigma_y\tau_y)/2$. When present, an electric potential difference V adds $\Delta\sigma_0\tau_z$ with $\Delta=V/2\hbar v$ to the Hamiltonian.

When $\gamma\gg\Delta$, it is convenient to eliminate the high energy degrees of freedom at $\pm\gamma$ to arrive at an effective low-energy two-band model (2) as follows:

$$\tilde{\mathcal{H}}_\nu=\boldsymbol{g}_\nu(\boldsymbol{q})\cdot\tilde{\boldsymbol{\sigma}}, \qquad [1]$$

where the $\tilde{\sigma}$ matrices act on two component spinors (ψ_{B_T},ψ_{A_B}) in the low-energy subspace for *AB* BLG and $\boldsymbol{g}_\nu(\boldsymbol{q})=(-(q_x^2-q_y^2)/\gamma, 2\nu q_xq_y/\gamma,\Delta)$. Eq. **1** admits a geometrical interpretation in which the negative energy eigenstates are spinors aligned with $-\boldsymbol{g}_\nu(\boldsymbol{q})$,

Author contributions: F.Z., A.H.M., and E.J.M. designed research; F.Z. and E.J.M. performed research; and F.Z., A.H.M., and E.J.M. wrote the paper.

The authors declare no conflict of interest.

[1]To whom correspondence should be addressed. E-mail: macd@physics.utexas.edu.

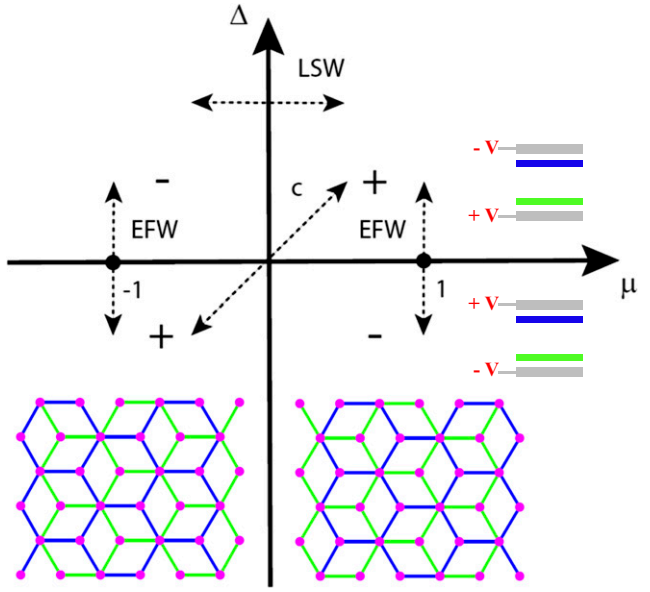

Fig. 1. A phase diagram illustrating the distinct valley-projected topological phases of BLG and the critical lines that separate them. A sign change of Δ denotes a reversal of the interlayer electric field. A sign change of μ denotes a transition from *AB* to *BA* interlayer registry. The spectrum is gapped except along the lines $\Delta = 0$ and $\mu = 0$.

and the filled band has a momentum space Berry curvature (13, 14) as follows:

$$\Omega_\nu(\boldsymbol{q}) = \frac{-2\nu\gamma\,\Delta\,q^2}{\left(q^4+\gamma^2\Delta^2\right)^{3/2}}. \qquad [2]$$

Because of the ν dependence in Eq. **2** the integral of $\Omega_\nu(\boldsymbol{q})$ over the full Brillouin zone is zero and the filled valence band carries total Chern number $N = 0$ as required by time reversal symmetry. However, for small Δ, the Berry curvature is strongly peaked at the gap minima near K and K'. Consequently, the integral of $\Omega_\nu(\boldsymbol{q})$ over an individual valley is accurately defined and the "valley Chern number" $N_\nu = -\nu\ \mathrm{sgn}(\Delta) = \pm 1$. The valley Chern number changes by $\Delta N_\nu = \pm 2$ across an EFW, which can be associated with the appearance of pairs of valley-projected edge modes copropagating along the boundary. These chiral modes have been obtained by analytic solution of the low-energy two-band model in the presence of a sharp EFW and by numerical solution for a spatially varying $\Delta(\boldsymbol{r})$ that smoothly connects two electric-field reversed states (12). As noted in previous work (13, 15), the introduction of a valley Chern number in this context is approximate because strictly speaking the construction does not map the full periodic Brillouin zone onto the parameter space of $\tilde{\mathcal{H}}_\nu$. Nonetheless, when Δ is small and intervalley scattering is absent the computed change ΔN_ν can be interpreted as a topological quantity, because $\Omega_\nu(\boldsymbol{q})$ is integrated over a closed surface produced by "gluing together" two integrals for the individual N_ν along a common boundary.

Layer Stacking Walls

We now turn to the case of a LSW at which the bilayer registry reverses from local *AB* to local *BA* with Δ held constant. Crossing a LSW changes the interlayer coupling matrix $\mathcal{H}_{int}$ and switches the orbitals that span its low-energy subspace. In this case, evaluation of the Berry curvature requires consideration of all four degrees of freedom in the bilayer Dirac problem. Alternatively, one can identity the topological origin of LSW modes by examining the residual phase twists induced at large momentum q in the eigenstates of the generalized Hamiltonian,

$$\mathcal{H}_{LSW} = \Delta\tau_z + \nu q_x\sigma_x + q_y\sigma_y + \frac{\gamma}{2}\left(\sigma_x\tau_x - \mu\sigma_y\tau_y\right), \qquad [3]$$

which reduces to the *AB* (*BA*) forms when $\mu \to 1(-1)$. For $q \gg |\Delta|, \gamma$ degenerate single layer states $\Psi_{\mu\nu}(\boldsymbol{q}) = (\psi_{\mu\nu,T}, \psi_{\mu\nu,B})$ deep in the filled band with energies $E = -|\boldsymbol{q}|$ are split by Δ and are mixed by γ in the projected Hamiltonian,

$$\mathcal{H}_\nu^- = -|q|\lambda_0 + \Delta\lambda_z - \frac{\nu\gamma}{4}\left(e^{i\mu\nu\phi}\lambda_+ + e^{-i\mu\nu\phi}\lambda_-\right), \qquad [4]$$

where $\boldsymbol{\lambda}$ are 2×2 Pauli matrices acting in the $\Psi_{\mu\nu}$ subspace and $\phi = \arctan(q_y/q_x)$. For large q, the eigenstates $\Psi_{\mu\nu,\pm}$ written in the original four orbital basis are as follows:

$$\Psi_{\mu\nu,\pm} = \frac{e^{i\alpha_{\mu\nu,\pm}(\phi)}}{2}\begin{pmatrix} \sqrt{1\pm\frac{\Delta}{\xi}} \\ \nu\sqrt{1\pm\frac{\Delta}{\xi}}\,e^{i\nu\phi} \\ \mp\nu\sqrt{1\mp\frac{\Delta}{\xi}}\,e^{-i\mu\nu\phi} \\ \mp\sqrt{1\mp\frac{\Delta}{\xi}}\,e^{i(1-\mu)\nu\phi} \end{pmatrix}, \qquad [5]$$

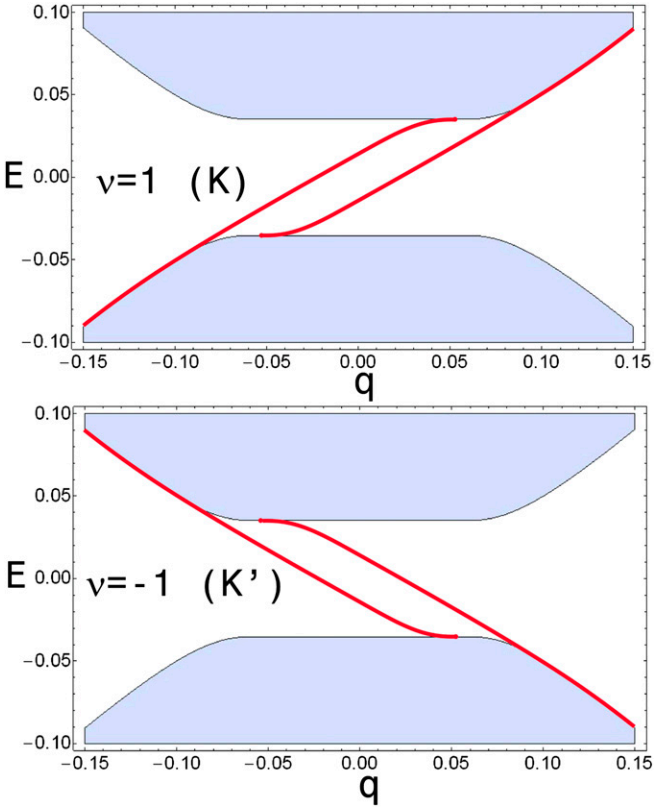

Fig. 2. Propagating chiral boundary modes (red) near the *K* (*Upper*) and *K'* (*Lower*) points calculated using the four-band continuum model for a domain wall separating regions with local *AB* and *BA* stacking registry in the presence of a uniform layer-potential difference Δ. The shaded regions show the support of the continuous bulk spectrum as a function of momentum $\boldsymbol{q}$ parallel to the domain wall. The results were obtained for the parameter values $\Delta = 0.05$, $\gamma = 0.1$.

PHYSICS

where $\xi = \sqrt{\gamma^2/4 + \Delta^2}$, and we explicitly display the overall $U(1)$ phases $\alpha_{\mu\nu,\pm}$. Using Eq. **5**, we calculate the momentum space Berry connection as follows:

$$\mathcal{A}_{\mu\nu,\pm} = \mathrm{Im}\,\langle \psi_\pm | \partial_\phi \psi_\pm \rangle = \frac{(1-\mu)\nu}{2} \pm \frac{\mu\nu\Delta}{2\xi} + \frac{\partial \alpha_{\mu\nu,\pm}}{\partial\phi}. \quad [6]$$

The change in the valley Chern numbers upon passing from the $\mu = 1$ to $\mu = -1$ states is obtained from the loop integral of the trace of $-\mu\mathcal{A}_{\mu\nu,\pm}$ over μ and band indices $\pm$, which reads as follows:

$$\Delta N_\nu = 2\,\nu + m_{-1,\nu,+} + m_{-1,\nu,-} - m_{1,\nu,+} - m_{1,\nu,-}. \quad [7]$$

Here, $m_{\mu\nu,\pm}$ are integer valued winding numbers of the overall phases $\alpha_{\mu\nu,\pm}$. The Δ dependence of this result vanishes after tracing over the filled bands, demonstrating that the valley Chern number in BLG is shared among all of the occupied bands rather than being confined just to its low-energy states as is often assumed. ΔN_ν is a topological index provided that the difference is evaluated in the same gauge for the two bounding phases, which requires that $m_{-1,\nu,\pm} = m_{1,\nu,\pm}$ for this boundary. It follows that $\Delta N_\nu = 2\,\nu$ and therefore that a domain wall separating insulating regions with local *AB* and *BA* registry will also confine pairs of valley-projected chiral modes propagating along the boundary with opposite velocities in the two valleys. Fig. 2 confirms this result by showing the spectra calculated by matching the full four-component wave functions of Eq. **3** across a sharp boundary where μ switches from 1 to −1.

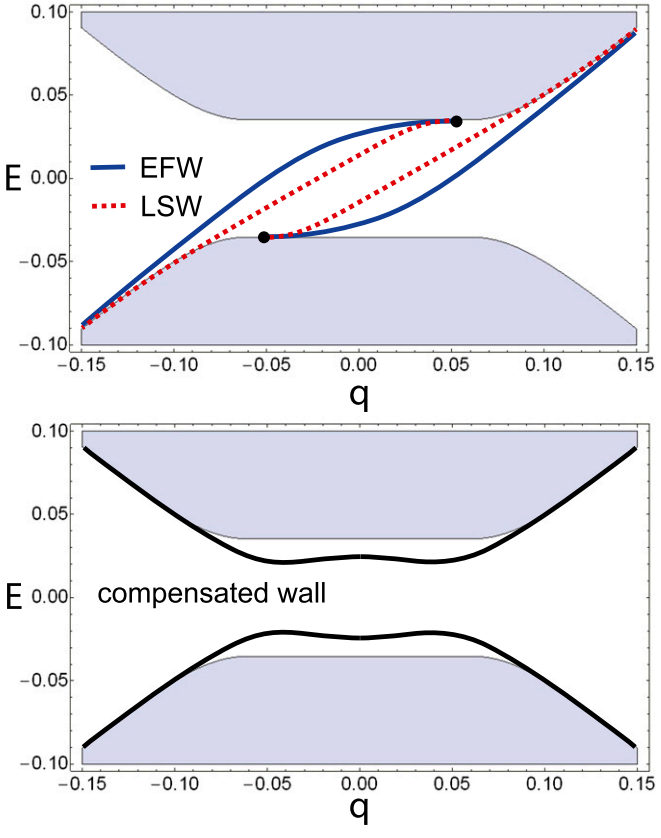

Fig. 3. (*Upper*) Comparison of valley *K* domain wall spectra for electric-field and layer-stacking walls. Both walls support a pair of copropagating chiral modes. (*Lower*) Interface spectrum calculated with a four-band theory for a topologically compensated boundary at which both layer stacking and electric field change sign. In this case, the boundary spectrum is completely gapped even in a continuum model.

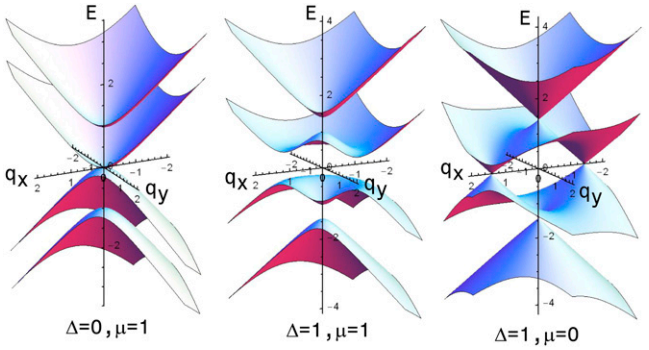

Fig. 4. Bulk band structures of three forms of BLG. (*Left*) BLG with uniform AB registry and no interlayer electric field characterized by quadratic touching between its two low energy bands. (*Center*) The field-induced gapped phase in which the BLG degeneracy is lifted by an interlayer electric field. (*Right*) A critical state with nonzero interlayer electric field where gap closure occurs at $\mu = 0$ as BLG crosses from *AB* to *BA* registry. The zero energy gap closures in the left and right panels separate four distinct gapped phases of BLG as shown in Fig. 1.

Using Eq. **5**, we find that at large q the wave functions on the two sides of the LSW are related by a gauge transformation,

$$\Psi_{\mu,\pm} \mapsto e^{i\mu\nu(1-\tau_z)\phi}\Psi_{\mu,\pm}, \quad [8]$$

with a different phase twist induced in each layer. It follows from the accumulation of internal phases in the two layers that $\Delta N_\nu = 2\mu\nu$. EFW walls, where the sign of the potential difference between layers Δ switches but the atomic registry μ does not change, can be analyzed similarly. Although Δ does not appear explicitly in ΔN_ν in Eq. **7**, there is an implicit dependence through the $U(1)$ phase prefactors. We find the following:

$$\mathcal{H}_{LSW}(-\Delta,\mu) = \tau_x\,\mathcal{H}_{LSW}(\Delta,-\mu)\,\tau_x, \quad [9]$$

i.e., that a sign reversal in Δ can be absorbed in a sign change of μ combined with a change of basis. Using this construction, the negative-energy eigenstates at large $\boldsymbol{q}$ on the two sides of the EFW are related by the following $U(1)$ gauge transformation:

$$\Psi_{\mu,\pm} \mapsto \mp\nu e^{i\mu\nu\phi}\Psi_{\mu,\pm}, \quad [10]$$

which produces the same overall $\Delta N_\nu = 2\mu\nu$ for the EFW. Eqs. **8–10** compactly express the relationship between these two different types of domain wall in the four-band theory. This is also illustrated in Fig. 3, which compares the valley *K* spectra computed for an EFW and a LSW showing their common chiral boundary modes.

In the LSW case, unlike the EFW case, analyzing the continuity of wave functions across the interface requires consideration of all four bands. The common topological origin of the domain wall spectra therefore becomes apparent only in a four-band continuum theory. Nevertheless, by integrating out the high-energy bands at energies of $\sim \pm\gamma$, we are able to construct a two-band effective model away from the domain wall in which for either case ΔN_ν is assigned to a sign change of the Berry curvature of the lower band. In this approach, Eq. **1** reads $\boldsymbol{g}_\nu(\boldsymbol{q}) = (-(q_x^2 - q_y^2)/\gamma, 2\mu\nu q_x q_y/\gamma, \Delta)$ with $\tilde{\boldsymbol{\sigma}}$ layer Pauli matrices that act on different spinors in the $\mu = \pm 1$ cases: on (ψ_{B_T}, ψ_{A_B}) for $\mu = 1$ and on (ψ_{A_T}, ψ_{B_B}) for $\mu = -1$. Because of inversion symmetry breaking, the valence band acquires a momentum space Berry curvature (13, 14),

$$\Omega_\nu(\boldsymbol{q}) = \frac{-2\mu\nu\gamma\ \Delta\ q^2}{\left(q^4+\gamma^2\Delta^2\right)^{3/2}}, \qquad [11]$$

which integrates over a single valley to $-\mu\nu\mathrm{sgn}(\Delta)$. Obviously, the valley Chern number changes by two across either an EFW or a LSW. Based on the bulk-boundary correspondence, pairs of valley-projected edge modes should copropagate along the interface.

Phase Diagram

The $\Delta-\mu$ plane phase diagram in Fig. 1 identifies distinct BLG topological phases. Phase boundaries occur along the μ and Δ axes where the spectrum of $\mathcal{H}_{LSW}(\Delta,\mu)$ undergoes gap closures at $E=0$. $\mathcal{H}_{LSW}(\Delta=0,\mu=1)$ describes an ungapped BLG system in which quadratic band crossing occurs exactly at $\boldsymbol{q}=0$, as seen in Fig. 4, *Left*. The gaps that open for the case of $\Delta\neq 0$ and $\mu=\pm 1$ are the electric field induced gaps easily understood within a two-band model. The boundary with $\Delta\neq 0$ and $\mu=0$ also has a gap closure, but it occurs at two finite momenta $q_x=\pm\sqrt{\Delta^2+\gamma^2/4}$ along the $q_y=0$ line where band crossing is possible because σ_x is a constant of the motion. For deviations in either q_x or q_y, the degeneracies at the band-crossing points are lifted at linear order, implying the conical gap closure illustrated in Fig. 4, *Right*. When $\mu\neq\pm 1$, the original quadratic gap closure fissions into a pair of linear Dirac singularities each of which carries one-half of the original winding number. Trajectories in the Hamiltonian parameter space that connect these topologically distinct ground states and involve different parameter values can shift the momenta at which the gap closures occur, but cannot eliminate them. For example, when $\Delta\neq 0$ but $\gamma=0$ in Eq. **3** the layers decouple and the gap closure at $E=0$ degenerates to a closed Fermi ring with radius Δ.

Fig. 1 also illustrates the possibility of a third type of compensated domain structure (labeled c) at which both the layer registry and interlayer electric field are reversed. Variation of local band parameters along this line connects two bilayer states that are distinct but have $\Delta N_\nu=0$. As illustrated in Fig. 3, *Lower*, spectra obtained by matching solutions across this compensated domain wall demonstrate that it hosts two pairs counter propagating modes within the same valley, which hybridize and completely gap the spectrum.

Fragility of Boundary Modes

The continuum model is able to explain the topological origin of the gapless interface modes. However, the short-range physics near the domain wall, which may be of essential significance, is not captured in the continuum Hamiltonian. Importantly, the single-valley physics that protects the chiral domain wall solutions can be preempted by sufficiently strong large-momentum scattering that acts to recouple states in the two valleys. In fact, Fig. 2 suggests that these single-valley domain wall modes ultimately reconnect with each other. What is critical is whether valley is a good quantum number. If it is not in the bulk, then there is no well defined topological invariant even at low-energy. If it is broken on the boundary, then there are no well controlled physical consequences even if one can define the bulk invariant. To study this further, we construct a specific lattice model and use it to investigate how both lattice and interfacial effects, which couple the two valleys, influence the domain wall modes.

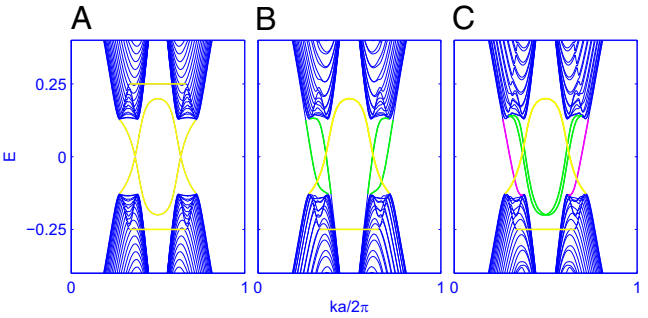

Fig. 6. Gapless modes for (*A*) uniform gapped BLG, for (*B*) gapped BLG with an EFW, and for (*C*) gapped BLG with a LSW as depicted in Fig. 5. The yellow states localize on the outer zigzag boundary and they are doubly degenerate in *B* and *C*. The green states localize on the EFW in *B* and on the LSW in *C*. In *C*, the green (magenta) LSW states localize on the broken (continuous) layer. To illustrate these different cases, we chose the following parameter values: $t=1$, $\gamma_1=0.3$, and $V/2=0.25$.

As depicted in Fig. 5, we consider the simplest LSW, i.e., a grain boundary separating BLG into left and right domains. Near the LSW, the lattices are continuous in one layer but fractured along a zigzag edge in the other. This introduces additional zigzag boundaries in the broken layer and allows switching of the bulk stacking order from B_TA_B ($\mu=-1$) on the left to A_TB_B ($\mu=1$) on the right. For comparison, we first calculate the band structures for the case of uniform gapped BLG and for the case of gapped BLG with an EFW at which stacking order is preserved. As expected and shown in Fig. 6 *A* and *B*, quantum valley Hall edge states (13) and two flat bands appear at the outer zigzag edges in uniformly gapped BLG. In the sample with an EFW, there is an additional pair of copropagating chiral gapless modes, which emerge at each valley. Fig. 6*C* shows the situation for a LSW with a uniform interlayer electric field; surprisingly, there are three instead of two gapless modes per valley in this case.

We investigate this problem further by studying the dependence on the tunneling amplitude t_c across the LSW shown as the dashed lines in Fig. 5. Without tunneling (Fig. 7*A*), the boundary mode spectrum yields two copies of the gapped BLG spectrum shown in Fig. 6*A*, and thus there are two chiral gapless modes in each valley as anticipated by the continuum model. The flat bands represent the states localized on the grain boundary lines B_B^{LI} and A_B^{RI} in Fig. 5. The leading effect of turning on the tunneling is that the pair of degenerate flat bands (magenta bands in Fig. 7) are split and become dispersive, as described in Fig. 7 *B* and *C*. When the tunneling is larger than the electric field induced gap, the flat band split downward is pushed down to the valence band and becomes the third gapless mode shown in Fig. 6*C*.

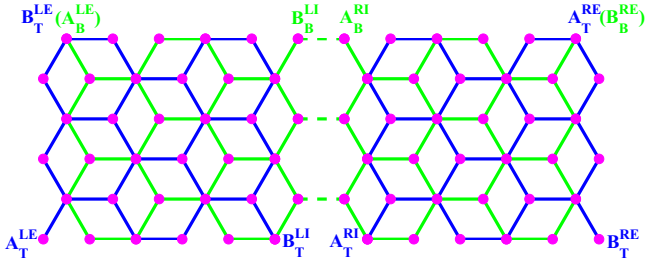

Fig. 5. The simplest LSW separating BLG into a left (L) domain with B_TA_B stacking ($\mu=-1$) and a right (R) domain with A_TB_B stacking ($\mu=1$). When the BLG is uniformly gapped, gapless modes emerge along the outer zigzag edges (E) as well as along the LSW interfaces (I). The lattices are continuous in the bottom (B) layer but have a straight crack in the top (T) layer. The dashed lines denote the tunneling between the domains within the continuous layer.

PHYSICS

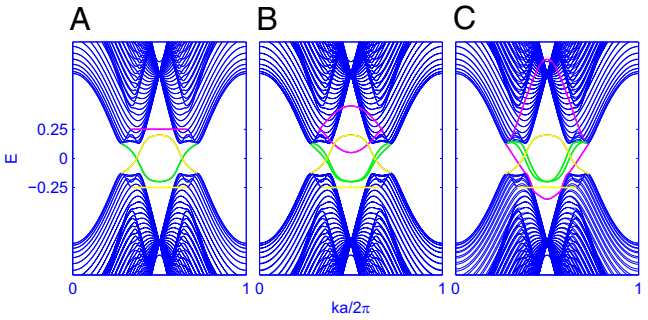

Fig. 7. Evolution of gapless modes for gapped BLG as a function of hybridization across the LSW. The tunneling parameter t_c is, respectively, 0 in *A*, 0.2 in *B*, 0.6 in *C*, and 1 in Fig. 6*C*. The other parameters have the same values as in Fig. 6. In *A*, all of the yellow, green, and magenta states are doubly degenerate.

The other two gapless modes (green bands in Fig. 7) localized on the grain boundary of the broken layer are almost degenerate due to the inversion symmetry between the lines B_T^{LI} and A_T^{RI} in Fig. 5. This degeneracy is exact at $ka=\pi$ and can be lifted by breaking the inversion symmetry between the left and right domains. We further find that a local potential U_{loc} on B_T^{LI} or A_T^{RI} can raise and lower the energies of the green bands. Similarly, a line potential on B_B^{LI} or A_B^{RI} can change the energies of the magenta bands. In view of these results we propose a criterion controlled by a hierarchy of energy scales to determine the number of fragile gapless modes in the atomically abrupt LSW shown in Fig. 5:

$$U_{loc}-\frac{V}{2}<-\frac{\Delta_{gap}}{2}, \qquad [12]$$

$$U_{loc}+\frac{V}{2}\pm t_c<-\frac{\Delta_{gap}}{2}, \qquad [13]$$

where $\Delta_{gap}/2$ is one-half size of the field-induced gap, which saturates if V exceeds a critical value (6). As described in Fig. 7*A*, the two green bands are independent of t_c and connect the two valleys at energy of $\sim -V/2$. When a positive (negative) U_{loc} on B_T^{LI} or A_T^{RI} is turned on, the corresponding green band will respond by shifting in energy. Eq. **12** is therefore the condition for the appearance of this gapless channel. The two magenta bands also connect the two valleys and become flat at energy $\sim V/2$ when $t_c=0$. Turning on t_c will lift their degeneracy and pin their energies to $V/2\pm t_c$ at $ka=\pi$. As in the case for green bands, a positive (negative) U_{loc} on B_B^{LI} or A_B^{RI} could move one magenta band upward (downward) whose emergence in the gap is related to fulfilling Eq. **13**.

When the LSW is made smooth in the sense that it does not produce sufficiently strong intervalley coupling, the tunneling amplitudes near the domain wall in both layers are almost the same as the pristine ones. In such a case, the tunneling between the left and right domains in the broken (continuous) layer would strongly split the two green (magenta) bands at $ka=\pi$. As a result, only one green and one magenta bands in Fig. 7 survive in the band gap, recovering our earlier continuum results.

Discussion

This article provides a general framework for understanding valley-projected chiral domain wall modes in BLG and their fate in the presence of possible lattice-scale potentials that acts to recouple states in the two valleys. We conclude that gapless interface modes at a LSW are topologically stable when the potential difference between layers is the dominant energy scale and the valley index can be regarded as a good quantum number. In this case, the valley Chern number provides a useful index for interpreting the valley-projected spectra. Domain walls where the electric field is reversed and where the layer stacking is reversed each induce phase twists in the manifold of occupied states, which, although distinct in these two situations, confine pairs of valley-projected chiral modes in the domain wall. Interestingly, even in the valley-projected problem, these modes can be gapped by their interaction within defects where both the perpendicular field and stacking order are allowed to vary in space. Furthermore, the topological protection of the domain wall modes can be preempted entirely by sufficiently strong lattice-scale physics. In this situation, the valley Chern number no longer characterizes the spectral properties and in the general case the number of domain wall modes can be any integer from 0 to 4 depending on the criteria like that implied by Eqs. **12** and **13**. The valley-projected topological-state analysis of BLG is illustrative of similar physics that occurs in all chiral multilayer graphene systems (6, 13) and is sensitive to stacking order, and to perpendicular electric fields.

ABA-ABC stacking domain walls are occasionally obtained in exfoliated trilayer graphene samples (20) and similar LSWs in bilayer and thicker chiral graphene are also experimentally accessible. A key difference is that the weak topological invariant (valley Chern number) cannot be defined on the ABA trilayer domain where the system is not gapped (20) even under a large perpendicular electric field. LSWs can be imaged by transmission electron microscopy, visualized by optical microscopy, and probed by scanning tunneling microscopy (STM) and transport experiments. When the STM tip crosses the LSW, sharp field-induced features in the local density of state at the gap edges should be suppressed due to the dispersive domain wall modes. In the presence of a perpendicular electric field, the conductance in a sample with a single LSW depends very sensitively on the orientation of the sample and on the positions of the contacts. Along a LSW, the Landauer conductance, in the absence of intervalley scattering, may reach Ne^2/h, where N is the number of nearly perfect transmission channels (17) in each valley. In a sample with many LSWs or with strong intervalley scattering, the conductance may be much smaller than e^2/h due to backscattering within and between the LSWs.

Note Added in Proof. After the completion of this work, a complementary preprint (21) and an experimental study (22) which cover closely related material have appeared.

ACKNOWLEDGMENTS. This work is supported by Defense Advanced Research Planning Agency under Grant SPAWAR N66001-11-1-4110, by the Department of Energy, Office of Basic Energy Sciences, under Contract DE-FG02-ER45118, and by The Welch Foundation Grant TBF1473.

1. Min H, MacDonald AH (2008) Chiral decomposition in the electronic structure of graphene multilayers. *Phys Rev B* 77:155416.
2. McCann E, Fal'ko VI (2006) Landau-level degeneracy and quantum Hall effect in a graphite bilayer. *Phys Rev Lett* 96(8):086805.
3. Ohta T, Bostwick A, Seyller T, Horn K, Rotenberg E (2006) Controlling the electronic structure of bilayer graphene. *Science* 313(5789):951–954.
4. Oostinga JB, Heersche HB, Liu X, Morpurgo AF, Vandersypen LMK (2008) Gate-induced insulating state in bilayer graphene devices. *Nat Mater* 7(2):151–157.
5. Castro EV, et al. (2007) Biased bilayer graphene: Semiconductor with a gap tunable by the electric field effect. *Phys Rev Lett* 99(21):216802.
6. Zhang F, Sahu B, Min H, MacDonald AH (2010) Band structure of ABC-stacked graphene trilayers. *Phys Rev B* 82:035409.
7. Zhang F, Min H, Polini M, MacDonald AH (2010) Spontaneous inversion symmetry breaking in graphene bilayers. *Phys Rev B* 81:041402.
8. Feldman BE, Martin J, Yacoby A (2009) Broken-symmetry states and divergent resistance in suspended bilayer graphene. *Nat Phys* 5:889–893.
9. Martin J, Feldman BE, Weitz RT, Allen MT, Yacoby A (2010) Local compressibility measurements of correlated states in suspended bilayer graphene. *Phys Rev Lett* 105(25):256806.
10. Velasco J, Jr., et al. (2012) Transport spectroscopy of symmetry-broken insulating states in bilayer graphene. *Nat Nanotechnol* 7(3):156–160.

11. Bao W, et al. (2012) Evidence for a spontaneous gapped state in ultraclean bilayer graphene. *Proc Natl Acad Sci USA* 109(27):10802–10805.
12. Martin I, Blanter YM, Morpurgo AF (2008) Topological confinement in bilayer graphene. *Phys Rev Lett* 100(3):036804.
13. Zhang F, Jung J, Fiete GA, Niu Q, MacDonald AH (2011) Spontaneous quantum Hall states in chirally stacked few-layer graphene systems. *Phys Rev Lett* 106(15): 156801.
14. Xiao D, Chang MC, Niu Q (2010) Berry phase effects on electronic properties. *Rev Mod Phys* 82:1959–2007.
15. Li J, Morpurgo AF, Büttiker M, Martin I (2010) Marginality of bulk-edge correspondence for single-valley Hamiltonians. *Phys Rev B* 82:245404.
16. Li J, Martin I, Buttiker M, Morpurgo AF (2011) Topological origin of subgap conductance in insulating bilayer graphene. *Nat Phys* 7:38.
17. Qiao Z, Jung J, Niu Q, Macdonald AH (2011) Electronic highways in bilayer graphene. *Nano Lett* 11(8):3453–3459.
18. Jung J, Zhang F, Qiao Z, MacDonald AH (2011) Valley-Hall kink and edge states in multilayer graphene. *Phys Rev B* 84:075418.
19. Zarenia M, Pereira JM, Jr., Farias GA, Peeters FM (2011) Chiral states in bilayer graphene: Magnetic field dependence and gap opening. *Phys Rev B* 84:125451.
20. Zou K, Zhang F, Clapp C, MacDonald AH, Zhu J (2013) Transport studies of dual-gated ABC and ABA trilayer graphene: Band gap opening and band structure tuning in very large perpendicular electric fields. *Nano Lett* 13(2):369–373.
21. Vaezi A, Liang Y, Ngai DH, Yang L, Kim E (2013) Topological kink states at a tilt boundary in gated multilayer graphene. arXiv:1301.1690.
22. Alden JS, et al. (2013) Strain solitons and topological defects in bilayer graphene. *Proc Natl Acad Sci USA*, 10.1073/pnas.1309394110.